ICES REPORT 16-12

May 2016

Stability of Multirate Explicit Coupling of Geomechanics with Flow in a Poroelastic Medium

by

Tameem Almani, Kundan Kumar, Gurpreet Singh, Mary F. Wheeler

The Institute for Computational Engineering and Sciences
The University of Texas at Austin
Austin, Texas 78712

Reference: Tameem Almani, Kundan Kumar, Gurpreet Singh, Mary F. Wheeler, "Stability of Multirate Explicit Coupling of Geomechanics with Flow in a Poroelastic Medium," ICES REPORT 16-12, The Institute for Computational Engineering and Sciences, The University of Texas at Austin, May 2016.

Stability of multirate explicit coupling of geomechanics with flow in a poroelastic medium

T. Almani[1], K. Kumar[2], G. Singh[1], M. F. Wheeler[1]
[1] Center for Subsurface Modeling, ICES, UT Austin, USA
[2] Mathematics Institute, University of Bergen, Norway
{tameem,gurpreet,mfw}@ices.utexas.edu, kundan.kumar@uib.no

May 11, 2016

Abstract

We consider single rate and multirate explicit schemes for the Biot system modeling coupled flow and geomechanics in a poro-elastic medium. These schemes are the most widely used in practice that follows a sequential procedure in which the flow and mechanics problems are fully decoupled. In such a scheme, the flow problem is solved first with time-lagging the displacement term followed by the mechanics solve. The multirate explicit coupling scheme exploits the different time scales for the mechanics and flow problems by taking multiple finer time steps for flow within one coarse mechanics time step. We provide fully discrete schemes for both the single and multirate approaches that use Backward Euler time discretization and mixed spaces for flow and conformal Galerkin for mechanics. We perform a rigorous stability analysis and derive the conditions on reservoir parameters and the number of finer flow solves to ensure stability for both schemes. Furthermore, we investigate the computational time savings for explicit coupling schemes against iterative coupling schemes.

Keywords. poroelasticity; Biot; iterative and explicit coupling; multirate scheme; mixed formulation

1 Introduction

The coupling between subsurface flow and reservoir geomechanics plays a critical role in obtaining accurate results for models involving reservoir deformation, surface subsidence, well stability, sand production, waste deposition, hydraulic fracturing, CO_2 sequestration, and hydrocarbon recovery [2, 8, 14]. The quasi-static Biot equations are used to model the subsurface coupled flow and mechanics and consists of a system of two coupled linear partial differential equations, each of which is typically associated with the flow and mechanics, respectively. Quite often in practice, the geomechanics problem has a much slower evolution than that of the flow problem. In such cases, the mechanics problem can cope with a much coarser time step compared to the flow problem. The multirate scheme exploits this difference in the two equations and allows the flow to take several finer time steps before updating the mechanics and is a natural candidate in this setting. Figures 1.1a and

1.1b illustrate the differences between single rate versus multirate explicit coupling schemes. Figure 1.1a represents a typical single rate scheme, in which the flow and mechanics problems share the exact same time step. In contrast, Figure 1.1b demonstrates a typical multirate scheme, in which the flow problem takes multiple finer local time steps within one coarser mechanics time step.

The explicit coupling approach that we consider here is the most widely utilized scheme in practice. The decoupling of the two equations makes it easy to implement and the time marching without any iterations leads to a lower computational cost. The drawback is that this scheme is only conditionally stable. For the single rate scheme, the rigorous stability properties have been investigated in the work of Mikelić and Wheeler [15]. However, in the case when the multiple flow time steps are taken for one mechanics time step, it is unclear how these stability properties change. In this work, we focus our attention on the explicit coupling approach, establish its stability theoretically for both fully discrete single rate and multirate schemes, and investigate its computational time savings numerically. Moreover, in contrast to the explicit coupling approach, the iterative coupling approach has been investigated in the past. In this approach, the two coupled subsystems are solved iteratively by exchanging the values of the shared state variables in an iterative manner. The procedure is iterated at each time step until the solution is obtained with an acceptable tolerance [5, 13, 14]. Multirate iterative coupling schemes, extending the fixed-stress split coupling algorithm, have been rigorously designed and analyzed in [1, 2]. Unconditional stability of such schemes follows immediately by establishing their Banach contraction properties. In addition, multirate iterative coupling schemes, based on the undrained-split coupling algorithm, are shown to be contractive, and thus unconditionally stable [12]. In this work, we consider explicit coupling schemes and rigorously establish their stability properties. In addition, we perform numerical computations on field scale problems to compare the efficiency and computational performance of these two approaches.

The coupled flow and geomechanics problem has been intensively investigated in the past pioneered by Terzaghi [21] and Biot [3, 4]. Terzaghi was the first to propose an explanation of the soil consolidation process, in which he assumed that grains forming the soil are bound together by some molecular forces resulting in the formation of the porous material with elastic properties. It is the success of Terzagh's theory in predicting the settlement of different types of soils that led to the creation of the science of soil mechanics [4]. Biot then extended Terzagh's one dimensional work to the three-dimensional case, and presented a more rigorous generalized theory of consolidation [4]. A comprehensive treatment of poromechanics and the theory of mechanics of porous continua can be found in [6] by Coussy. Other nonlinear extensions on the theory of poroelasticity can be found in [7, 17, 20].

Recently, the work of Mikelić and Wheeler [15] establishes stability and geometric convergence (contraction with respect to appropriately chosen metrics) for different flow and geomechanics coupling schemes. In addition, Kim et al. [10, 11] have used von Neumann stability analysis to study the stability and convergence of similar schemes. The multirate schemes for the non-stationary Stokes-Darcy model have been investigated in [18, 24]. In this work of multirate explicit coupling of flow with geomechanics, we establish stability results for both the single rate and multirate schemes, and investigate their accuracies and computational time savings numerically. To the best of our knowledge, this is the first

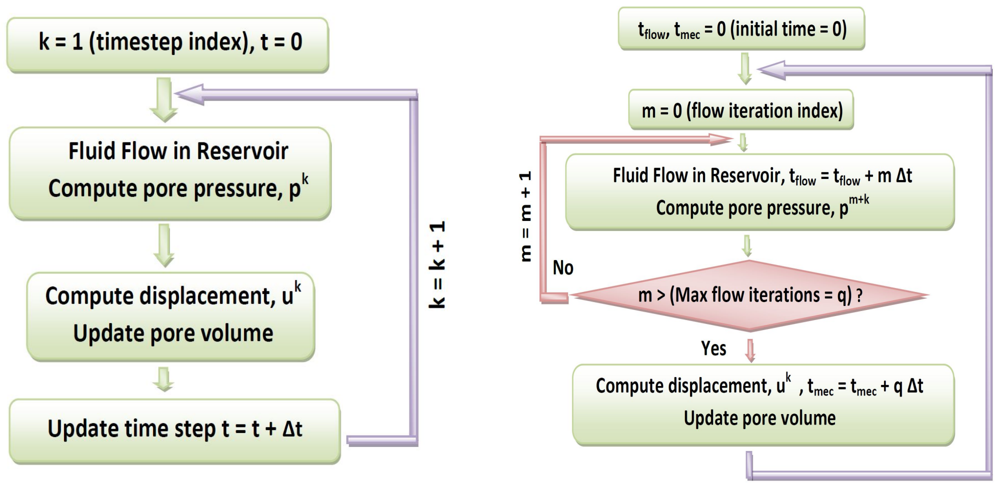

(a) Single Rate (b) Multirate

Figure 1.1: Flowchart for explicit single rate and multirate time stepping for coupled geomechanics and flow problem

analysis of the multirate explicit coupling scheme for Biot equations.
The paper is structured as follows. We present the model and discretization in Section 2. The single rate and multirate explicit coupling schemes are introduced and analyzed in Section 3. Numerical results are shown in Section 4. Conclusions and outlook are discussed in Section 5.

1.1 Preliminaries

Let Ω be a bounded domain (open and connected) of $I\!R^d$, where the dimension $d = 2$ or 3, with a Lipschitz continuous boundary $\partial\Omega$, and let Γ be a part of $\partial\Omega$ with positive measure. When $d = 3$, we assume that the boundary of Γ is also Lipschitz continuous. As usual, we denote by $H^1(\Omega)$ the classical Sobolev space

$$H^1(\Omega) = \{v \in L^2(\Omega)\,;\, \nabla\, v \in L^2(\Omega)^d\},$$

equipped with the semi-norm and norm:

$$|v|_{H^1(\Omega)} = \|\nabla\, v\|_{L^2(\Omega)^d} \quad , \quad \|v\|_{H^1(\Omega)} = (\|v\|^2_{L^2(\Omega)} + |v|^2_{H^1(\Omega)})^{1/2}.$$

We also define:

$$H^1_0(\Omega) = \{v \in H^1(\Omega)\,;\, v|_{\partial\Omega} = 0\},$$

and for the divergence operator, we shall use the space

$$H(\mathrm{div};\Omega) = \{\boldsymbol{v} \in L^2(\Omega)^d\,;\, \nabla\cdot\boldsymbol{v} \in L^2(\Omega)\},$$

equipped with the norm

$$\|\boldsymbol{v}\|_{H(\mathrm{div};\Omega)} = (\|\boldsymbol{v}\|^2_{L^2(\Omega)} + \|\nabla\cdot\boldsymbol{v}\|^2_{L^2(\Omega)})^{1/2}.$$

For a vector $\boldsymbol{v}$ in $I\!R^d$, recall the strain (or symmetric gradient) tensor $\boldsymbol{\varepsilon}(\boldsymbol{v})$:

$$\boldsymbol{\varepsilon}(\boldsymbol{v}) = \frac{1}{2}(\nabla \boldsymbol{v} + (\nabla \boldsymbol{v})^T).$$

In the sequel we shall use Poincaré's and Korn's inequalities. Poincaré's inequality in $H_0^1(\Omega)$ reads: There exists a constant $\mathcal{P}_\Omega$ depending only on Ω such that

$$\forall v \in H_0^1(\Omega)\,,\ \|v\|_{L^2(\Omega)} \leq \mathcal{P}_\Omega |v|_{H^1(\Omega)}. \tag{1.1}$$

Next, recall Korn's first inequality in $H_0^1(\Omega)^d$: There exists a constant C_κ depending only on Ω such that

$$\forall \boldsymbol{v} \in H_0^1(\Omega)^d\,,\ |\boldsymbol{v}|_{H^1(\Omega)} \leq C_\kappa \|\boldsymbol{\varepsilon}(\boldsymbol{v})\|_{L^2(\Omega)}. \tag{1.2}$$

2 Model equations, discretization and splitting algorithm

We assume a linear, elastic, homogeneous, and isotropic poro-elastic medium $\Omega \subset \mathbb{R}^d$, $d = 2$ or 3, in which the reservoir is saturated with a slightly compressible viscous fluid.

2.1 Assumptions

The fluid is assumed to be slightly compressible and its density is a linear function of pressure, with a constant viscosity $\mu_f > 0$. The reference density of the fluid $\rho_f > 0$, the Lamé coefficients $\lambda > 0$ and $G > 0$, the dimensionless Biot coefficient α, and the pore volume φ^* are all positive. The absolute permeability tensor, $\boldsymbol{K}$, is assumed to be symmetric, bounded, uniformly positive definite in space and constant in time.

A quasi-static Biot model [4, 8] will be employed in this work. The model reads: Find $\boldsymbol{u}$ and p satisfying the equations below for all time $t \in]0, T[$:

Flow Equation:

$$\frac{\partial}{\partial t}\Big((\tfrac{1}{M} + c_f\varphi_0)p + \alpha \nabla\cdot\boldsymbol{u}\Big) - \nabla\cdot\Big(\tfrac{1}{\mu_f}\boldsymbol{K}(\nabla p - \rho_{f,r} g \nabla \eta)\Big) = \tilde{q} \ \text{ in } \Omega$$

Mechanics Equations:

$$-\mathrm{div}\,\boldsymbol{\sigma}^{\mathrm{por}}(\boldsymbol{u}, p) = \boldsymbol{f} \ \text{ in } \Omega,$$
$$\boldsymbol{\sigma}^{\mathrm{por}}(\boldsymbol{u}, p) = \boldsymbol{\sigma}(\boldsymbol{u}) - \alpha\, p\, \boldsymbol{I} \ \text{ in } \Omega,$$
$$\boldsymbol{\sigma}(\boldsymbol{u}) = \lambda(\nabla\cdot\boldsymbol{u})\boldsymbol{I} + 2\,G\boldsymbol{\varepsilon}(\boldsymbol{u}) \ \text{ in } \Omega$$

Boundary Conditions:

$$\boldsymbol{u} = \boldsymbol{0}\ ,\ \boldsymbol{K}(\nabla p - \rho_{f,r} g \nabla \eta)\cdot\boldsymbol{n} = 0 \ \text{ on } \partial\Omega$$

Initial Condition $(t = 0)$:

$$\Big((\tfrac{1}{M} + c_f\varphi_0)p + \alpha\nabla\cdot\boldsymbol{u}\Big)(0) = (\tfrac{1}{M} + c_f\varphi_0)p_0 + \alpha\nabla\cdot\boldsymbol{u}_0.$$

where: g is the gravitational constant, η is the distance in the vertical direction (assumed to be constant in time), $\rho_{f,r} > 0$ is a constant reference density (relative to the reference pressure p_r), φ_0 is the initial porosity, M is the Biot constant, $\tilde{q} = \frac{q}{\rho_{f,r}}$ where q is a mass source or sink term taking into account injection into or out of the reservoir. We remark that the above system is linear and coupled through the Biot coefficient terms.

2.2 Mixed variational formulation

A mixed finite element formulation for flow and a conformal Galerkin formulation for mechanics will be used. The mixed formulation is a locally mass conservative scheme, and allows for explicit flux computation. The flux is defined as a separate unknown and the flow equation is rewritten as a system of first order equations. Accordingly, for the fully discrete formulation (discrete in time and space), we use a mixed finite element method for space discretization and a backward-Euler time discretization. Let $\mathfrak{T}_h$ denote a regular family of conforming triangular elements of the domain of interest, $\overline{\Omega}$. Using the lowest order Raviart-Thomas (RT) spaces , we have the following discrete spaces ($\boldsymbol{V}_h$ for discrete displacements, Q_h for discrete pressures, and $\boldsymbol{Z}_h$ for discrete velocities (fluxes)):

$$\boldsymbol{V}_h = \{\boldsymbol{v}_h \in H^1(\Omega)^d \, ; \, \forall T \in \mathfrak{T}_h, \boldsymbol{v}_{h|T} \in \mathbb{P}_1{}^d, \boldsymbol{v}_{h|\partial\Omega} = \boldsymbol{0}\} \tag{2.1}$$

$$Q_h = \{p_h \in L^2(\Omega) \, ; \, \forall T \in \mathfrak{T}_h, p_{h|T} \in \mathbb{P}_0\} \tag{2.2}$$

$$\boldsymbol{Z}_h = \{\boldsymbol{q}_h \in H(\mathrm{div};\Omega)^d \, ; \forall T \in \mathfrak{T}_h, \boldsymbol{q}_{h|T} \in \mathbb{P}_1{}^d, \, \boldsymbol{q}_h \cdot \boldsymbol{n} = 0 \text{ on } \partial\Omega\} \tag{2.3}$$

The space of displacements, $\boldsymbol{V}_h$, is equipped with the norm:

$$\|\boldsymbol{v}\|_{V_h} = (\sum_{i=1}^{d} \|v_i\|^2_{\Omega})^{1/2}.$$

We also assume that the finer time step is given by: $\Delta t = t_k - t_{k-1}$. If we denote the total number of timesteps by N, then the total simulation time is given by T = Δt N, and $t_i = i\Delta t$, $0 \leqslant i \leqslant N$ denote the discrete time points.

For the fully discrete scheme, we have chosen the Raviart-Thomas spaces for the mixed finite element discretization. However, the proof extends to other choices for the mixed spaces, and we will state the results for Multipoint Flux Mixed Finite Element (MFMFE) spaces [23] in Remark 3.6.

Remark 2.1 Notation: *We adopt the following notations,k denotes the coarser time step iteration index (for indexing mechanics coarse time steps), m is the finer (local) time step iteration index (for indexing flow fine time steps),* Δt *stands for the unit (finer) time step, and q is the "fixed" number of local flow time steps per coarse mechanics time step.*

2.3 Fully discrete scheme for single rate

As discussed above, using the mixed finite element method in space and the backward Euler finite difference method in time, the weak formulation of the single rate scheme reads as follows.

Definition 2.2 *(**flow equation**) Find $p_h^{k+1} \in Q_h$, and $\boldsymbol{z}_h^{k+1} \in \boldsymbol{Z}_h$ such that,*

$$\forall \theta_h \in Q_h, (\frac{1}{M} + c_f \varphi_0)\Big(\frac{p_h^{k+1} - p_h^k}{\Delta t}, \theta_h\Big) + \frac{1}{\mu_f}\Big(\nabla \cdot \boldsymbol{z}_h^{k+1}, \theta_h\Big) + \alpha\Big(\nabla \cdot \frac{\boldsymbol{u}_h^k - \boldsymbol{u}_h^{k-1}}{\Delta t}, \theta_h\Big) = \Big(\tilde{q}_h, \theta_h\Big) \tag{2.4}$$

$$\forall \boldsymbol{q}_h \in \boldsymbol{Z}_h, \Big(K^{-1} \boldsymbol{z}_h^{k+1}, \boldsymbol{q}_h\Big) = \Big(p_h^{k+1}, \nabla \cdot \boldsymbol{q}_h\Big) + \Big(\nabla(\rho_{f,r} g \eta), \boldsymbol{q}_h\Big) \tag{2.5}$$

Definition 2.3 *(**mechanics equation**) Find $\boldsymbol{u}_h^{k+q} \in \boldsymbol{V}_h$ such that,*

$$\forall \boldsymbol{v}_h \in V_h, 2G(\boldsymbol{\varepsilon}(\boldsymbol{u}_h^{k+1}), \boldsymbol{\varepsilon}(\boldsymbol{v}_h)) + \lambda(\nabla \cdot \boldsymbol{u}_h^{k+1}, \nabla \cdot \boldsymbol{v}_h) - \alpha(p_h^{k+1}, \nabla \cdot \boldsymbol{v}_h) = \Big(\boldsymbol{f}_h^{k+1}, \boldsymbol{v}_h\Big) \tag{2.6}$$

2.4 Fully discrete scheme for multirate

The weak formulation of the multirate scheme reads as follows.

Definition 2.4 *(**flow equation**) For $1 \leq m \leq q$, find $p_h^{m+k} \in Q_h$, and $\boldsymbol{z}_h^{m+k} \in \boldsymbol{Z}_h$ such that,*

$$\begin{aligned} \forall \theta_h \in Q_h \,, \frac{1}{\Delta t}\Big((\frac{1}{M} + c_f \varphi_0)\Big(p_h^{m+k} - p_h^{m-1+k}\Big), \theta_h\Big) + \frac{1}{\mu_f}(\nabla \cdot \boldsymbol{z}_h^{m+k}, \theta_h) = \\ - \frac{\alpha}{q \Delta t}\Big(\nabla \cdot \Big(\boldsymbol{u}_h^k - \boldsymbol{u}_h^{k-q}\Big), \theta_h\Big) + \Big(\tilde{q}_h, \theta_h\Big), \end{aligned} \tag{2.7}$$

$$\forall \boldsymbol{q}_h \in \boldsymbol{Z}_h \,, \Big(\boldsymbol{K}^{-1} \boldsymbol{z}_h^{m+k}, \boldsymbol{q}_h\Big) = \Big(p_h^{m+k}, \nabla \cdot \boldsymbol{q}_h\Big) + \Big(\rho_{f,r} g \nabla \eta, \boldsymbol{q}_h\Big), \tag{2.8}$$

Definition 2.5 *(**mechanics equation**) Find $\boldsymbol{u}_h^{k+q} \in \boldsymbol{V}_h$ such that,*

$$\forall \boldsymbol{v}_h \in V_h \,, 2G(\boldsymbol{\varepsilon}(\boldsymbol{u}_h^{k+q}), \boldsymbol{\varepsilon}(\boldsymbol{v}_h)) + \lambda(\nabla \cdot \boldsymbol{u}_h^{k+q}, \nabla \cdot \boldsymbol{v}_h) - \alpha(p_h^{k+q}, \nabla \cdot \boldsymbol{v}_h) = (\boldsymbol{f}_h^{k+q}, \boldsymbol{v}_h). \tag{2.9}$$

with the initial condition for the first discrete time step (for both single rate and multirate schemes),

$$p_h^0 = p_0. \tag{2.10}$$

Note that for the multirate scheme, the pressure unknowns p_h and flux unknowns $\boldsymbol{z}_h$ are being solved at finer time steps $t_{k+m}, m = 0, \ldots, q$ whereas the mechanics variables $\boldsymbol{u}_h$ are being solved at $t_{iq}, i \in \mathbb{N}$. Therefore, for each mechanics time step of size $q\Delta t$, there are q flow solves justifying the nomenclature of multirate. Moreover, the above system of PDEs is linear, decoupled and the information exchange taking place at the coarse time steps.

3 Analysis of Explicit Coupling Schemes

In this section, we perform a mathematically rigorous analysis of the stability of the single rate and multirate explicit coupling schemes. Recall that in the single rate case (Figure 1.1a), the flow and mechanics problems share the exact same time step. In contrast, in the multirate case (Figure 1.1b), the flow problem takes q finer local time steps within one coarser mechanics time step. As has been stated above, the explicit coupling approach is a sequential procedure in which the flow or the mechanics problem is solved first followed by the other. There is no coupling iteration between the two problems.

3.1 Single Rate Formulation:

We start by analyzing the single-rate explicit coupling algorithm, in which both flow and mechanics share the same time step. To the best of our knowledge, this is the first rigorous mathematical analysis of the fully discrete single-rate explicitly coupled Biot system. In addition, the analysis reveals a more general stability condition compared to the one obtained in [16] by elementary means. The algorithm is given as follows:

Algorithm 1: Single Rate Explicit Coupling Algorithm

Given initial conditions $\boldsymbol{u}_h^0$ *and* p_h^0*, solve fully implicitly for* $p_h^1, \boldsymbol{u}_h^1$ *satisfying Biot model*

for $k = 1, 2, \ldots$ **do** `/* time step index */`

  First Step: Flow equations

  Given $\boldsymbol{u}_h^k$ *and* $\boldsymbol{u}_h^{k-1}$*:*

    Solve for p_h^{k+1} *and* $\boldsymbol{z}_h^{k+1}$ *satisfying definition 2.2*

  Second Step: Mechanics equations

  Given p_h^{k+1} *and,* $\boldsymbol{z}_h^{k+1}$*:*

    Solve for $\boldsymbol{u}_h^{k+1}$ *satisfying definition 2.3*

Note that we begin with $k = 1$ and we require both $\boldsymbol{u}_h^1$ and $\boldsymbol{u}_h^0$ for obtaining p_h^2. In the first step, we use a fully implicit method to solve for $p_h^1, \boldsymbol{u}_h^1$. Alternatively, to keep the problem decoupled, we can use iterative techniques such as fixed stress splitting or undrained splitting [15].

3.1.1 Assumptions

For notational convenience, we define

$$\beta = (\frac{1}{M} + c_f \varphi_0).$$

For stability to hold, we assume the following:

$$(\mathbf{A_1}) \quad \beta > \tfrac{\alpha^2}{\lambda}.$$

3.1.2 Result

Our results make explicit the dependence of the stability on the difference of the above quantities. we have the following stability result.

Theorem 3.1 *[Single rate] Under the Assumption* $\mathbf{A_1}$ *above, the following stability result holds for the single rate explicit coupling scheme for time steps* $t_0 \le t_k \le t_J$*:*

$$\frac{\Delta t}{\lambda \mu_f}\left(\left\|K^{-1/2}\boldsymbol{z}_h^{J+1}\right\|^2 + \sum_{k=1}^{J}\left\|K^{-1/2}(\boldsymbol{z}_h^{k+1} - \boldsymbol{z}_h^k)\right\|^2\right) + \frac{2G}{\lambda}\sum_{k=1}^{J}\left\|\boldsymbol{\varepsilon}(\boldsymbol{u}_h^{k+1} - \boldsymbol{u}_h^k)\right\|^2$$
$$+ \left\|\nabla\cdot(\boldsymbol{u}_h^{J+1} - \boldsymbol{u}_h^J)\right\|^2 \le C\Delta t + \frac{\Delta t^2}{2\lambda(\beta - \frac{\alpha^2}{\lambda})}\sum_{k=1}^{J}\left\|\tilde{q}_h\right\|^2 + \frac{\mathcal{P}_\Omega^2 C_\kappa^2}{2G\lambda}\sum_{k=1}^{J}\left\|\boldsymbol{f}_h^{k+1} - \boldsymbol{f}_h^k\right\|^2$$

3.1.3 Stability Analysis:

The proof of the above theorem is carried out in three steps by considering the flow equation, the mechanics equation and then combining the two together. Recall that $\beta = \frac{1}{M} + c_f \varphi_0$.
Proof.

- **Step 1: Flow equations**
  Testing (2.4) with $\theta_h = p_h^{k+1} - p_h^k$, we obtain

$$\beta \frac{1}{\Delta t} \left\| p_h^{k+1} - p_h^k \right\|^2 + \frac{1}{\mu_f} \left(\nabla \cdot \boldsymbol{z}_h^{k+1}, p_h^{k+1} - p_h^k \right) + \frac{\alpha}{\Delta t} \left(\nabla \cdot (\boldsymbol{u}_h^k - \boldsymbol{u}_h^{k-1}), p_h^{k+1} - p_h^k \right) = \left(\tilde{q}_h, p_h^{k+1} - p_h^k \right) \tag{3.1}$$

  Next, we consider the flux equation (2.5). Taking the difference of two consecutive time steps $t = t_{k+1}$ and $t = t_k$ and testing with $\boldsymbol{q}_h = \boldsymbol{z}_h^{k+1}$, we obtain:

$$\left(K^{-1} (\boldsymbol{z}_h^{k+1} - \boldsymbol{z}_h^k), \boldsymbol{z}_h^{k+1} \right) = \left(p_h^{k+1} - p_h^k, \nabla \cdot \boldsymbol{z}_h^{k+1} \right) \tag{3.2}$$

  Substituting (3.2) into (3.1), after some algebraic manipulations of the resulting term (using: $a(a-b) = \frac{1}{2}(a^2 - b^2 + (a-b)^2)$), we derive

$$\frac{\beta}{\Delta t} \left\| p_h^{k+1} - p_h^k \right\|^2 + \frac{1}{2\mu_f} \left(\left\| K^{-1/2} \boldsymbol{z}_h^{k+1} \right\|^2 - \left\| K^{-1/2} \boldsymbol{z}_h^k \right\|^2 + \left\| K^{-1/2} (\boldsymbol{z}_h^{k+1} - \boldsymbol{z}_h^k) \right\|^2 \right) + \frac{\alpha}{\Delta t} \left(\nabla \cdot \boldsymbol{u}_h^k - \boldsymbol{u}_h^{k-1}, p_h^{k+1} - p_h^k \right) = \left(\tilde{q}_h, p_h^{k+1} - p_h^k \right) \tag{3.3}$$

- **Step 2: Elasticity equation**
  Considering (2.6) for the difference of two consecutive time steps, $t = t_{k+1}$ and $t = t_k$, and testing with $\boldsymbol{v}_h = \frac{\boldsymbol{u}_h^{k+1} - \boldsymbol{u}_h^k}{\Delta t}$, we obtain

$$\frac{2G}{\Delta t} \left\| \boldsymbol{\varepsilon}(\boldsymbol{u}_h^{k+1} - \boldsymbol{u}_h^k) \right\|^2 + \frac{\lambda}{\Delta t} \left\| \nabla \cdot (\boldsymbol{u}_h^{k+1} - \boldsymbol{u}_h^k) \right\|^2 - \frac{\alpha}{\Delta t} \left(p_h^{k+1} - p_h^k, \nabla \cdot (\boldsymbol{u}_h^{k+1} - \boldsymbol{u}_h^k) \right) = \frac{1}{\Delta t} \left(\boldsymbol{f}_h^{k+1} - \boldsymbol{f}_h^k, \boldsymbol{u}_h^{k+1} - \boldsymbol{u}_h^k \right) \tag{3.4}$$

- **Step 3: Combining flow and elasticity equations**
  Combining (3.3) with (3.4) yields

$$
\begin{aligned}
&\frac{\beta}{\Delta t}\left\|p_h^{k+1}-p_h^k\right\|^2+\frac{1}{2\mu_f}\left(\left\|K^{-1/2}\boldsymbol{z}_h^{k+1}\right\|^2-\left\|K^{-1/2}\boldsymbol{z}_h^{k}\right\|^2+\left\|K^{-1/2}(\boldsymbol{z}_h^{k+1}-\boldsymbol{z}_h^{k})\right\|^2\right)\\
&+\frac{2G}{\Delta t}\left\|\boldsymbol{\varepsilon}(\boldsymbol{u}_h^{k+1}-\boldsymbol{u}_h^k)\right\|^2+\frac{\lambda}{\Delta t}\left\|\nabla\cdot(\boldsymbol{u}_h^{k+1}-\boldsymbol{u}_h^k)\right\|^2=\underbrace{-\frac{\alpha}{\Delta t}\left(\nabla\cdot(\boldsymbol{u}_h^{k}-\boldsymbol{u}_h^{k-1}),p_h^{k+1}-p_h^k\right)}_{R_1}\\
&+\underbrace{\frac{\alpha}{\Delta t}\left(p_h^{k+1}-p_h^k,\nabla\cdot(\boldsymbol{u}_h^{k+1}-\boldsymbol{u}_h^k)\right)}_{R_2}+\underbrace{\left(\tilde{q}_h,p_h^{k+1}-p_h^k\right)}_{R_3}+\underbrace{\frac{1}{\Delta t}\left(\boldsymbol{f}_h^{k+1}-\boldsymbol{f}_h^k,\boldsymbol{u}_h^{k+1}-\boldsymbol{u}_h^k\right)}_{R_4}
\end{aligned}
\tag{3.5}
$$

  Denoting by R_1, R_2, R_3, and R_4 the terms on the right hand side, together with Poincaré's, Korn's, and Young's inequalities, we estimate

$$
\begin{aligned}
|R_1|&\le\frac{\alpha}{\Delta t}\frac{1}{2\epsilon_1}\left\|\nabla\cdot(\boldsymbol{u}_h^{k}-\boldsymbol{u}_h^{k-1})\right\|^2+\frac{\alpha}{\Delta t}\frac{\epsilon_1}{2}\left\|p_h^{k+1}-p_h^k\right\|^2\\
|R_2|&\le\frac{\alpha}{2\Delta t\epsilon_2}\left\|\nabla\cdot(\boldsymbol{u}_h^{k+1}-\boldsymbol{u}_h^{k})\right\|^2+\frac{\alpha\epsilon_2}{2\Delta t}\left\|p_h^{k+1}-p_h^k\right\|^2\\
|R_3|&\le\frac{1}{2\epsilon_3}\left\|\tilde{q}_h\right\|^2+\frac{\epsilon_3}{2}\left\|p_h^{k+1}-p_h^k\right\|^2\\
|R_4|&\le\frac{1}{2\Delta t\epsilon_4}\left\|\boldsymbol{f}_h^{k+1}-\boldsymbol{f}_h^k\right\|^2+\frac{\epsilon_4}{2\Delta t}\left\|\boldsymbol{u}_h^{k+1}-\boldsymbol{u}_h^k\right\|^2\\
&\le\frac{1}{2\Delta t\epsilon_4}\left\|\boldsymbol{f}_h^{k+1}-\boldsymbol{f}_h^k\right\|^2+\frac{\epsilon_4\mathcal{P}_\Omega^2C_\kappa^2}{2\Delta t}\|\boldsymbol{\varepsilon}(\boldsymbol{u}_h^{k+1}-\boldsymbol{u}_h^k)\|^2.
\end{aligned}
$$

  for $\epsilon_1, \epsilon_2, \epsilon_3,$ and $\epsilon_4 > 0$. Choosing $\epsilon_1=\epsilon_2=\frac{\alpha}{\lambda}$, $\epsilon_3=\frac{2}{\Delta t}(\beta-\frac{\alpha^2}{\lambda})$, $\epsilon_4=\frac{2G}{\mathcal{P}_\Omega^2C_\kappa^2}$ and multiplying (3.5) by $\frac{2\Delta t}{\lambda}$, we derive

$$
\begin{aligned}
&\frac{\Delta t}{\lambda\mu_f}\left(\left\|K^{-1/2}\boldsymbol{z}_h^{k+1}\right\|^2-\left\|K^{-1/2}\boldsymbol{z}_h^{k}\right\|^2+\left\|K^{-1/2}(\boldsymbol{z}_h^{k+1}-\boldsymbol{z}_h^{k})\right\|^2\right)+\frac{2G}{\lambda}\left\|\boldsymbol{\varepsilon}(\boldsymbol{u}_h^{k+1}-\boldsymbol{u}_h^k)\right\|^2\\
&+\left\|\nabla\cdot(\boldsymbol{u}_h^{k+1}-\boldsymbol{u}_h^k)\right\|^2\le\left\|\nabla\cdot(\boldsymbol{u}_h^{k}-\boldsymbol{u}_h^{k-1})\right\|^2+\frac{\Delta t^2}{2\beta\lambda-2\alpha^2}\left\|\tilde{q}_h\right\|^2+\frac{\mathcal{P}_\Omega^2C_\kappa^2}{2G\lambda}\left\|\boldsymbol{f}_h^{k+1}-\boldsymbol{f}_h^k\right\|^2
\end{aligned}
\tag{3.6}
$$

  Summing up (3.6) for $1 \le k \le J$, for J time steps, with telescopic cancellations, we get:

$$
\begin{aligned}
&\frac{\Delta t}{\lambda\mu_f}\left(\left\|K^{-1/2}\boldsymbol{z}_h^{J+1}\right\|^2+\sum_{k=1}^{J}\left\|K^{-1/2}(\boldsymbol{z}_h^{k+1}-\boldsymbol{z}_h^{k})\right\|^2\right)+\frac{2G}{\lambda}\sum_{k=1}^{J}\left\|\boldsymbol{\varepsilon}(\boldsymbol{u}_h^{k+1}-\boldsymbol{u}_h^k)\right\|^2\\
&+\left\|\nabla\cdot(\boldsymbol{u}_h^{J+1}-\boldsymbol{u}_h^J)\right\|^2\le\left\|\nabla\cdot(\boldsymbol{u}_h^{1}-\boldsymbol{u}_h^{0})\right\|^2+\frac{\Delta t}{\lambda\mu_f}\left\|K^{-1/2}\boldsymbol{z}_h^1\right\|^2+\frac{\Delta t^2}{2\lambda(\beta-\frac{\alpha^2}{\lambda})}\sum_{k=1}^{J}\left\|\tilde{q}_h\right\|^2\\
&\qquad+\frac{\mathcal{P}_\Omega^2C_\kappa^2}{2G\lambda}\sum_{k=1}^{J}\left\|\boldsymbol{f}_h^{k+1}-\boldsymbol{f}_h^k\right\|^2,
\end{aligned}
\tag{3.7}
$$

Recall that $\boldsymbol{u}_h^1, \boldsymbol{z}_h^1$ have been computed using the fully implicit time discretization. Using standard a priori estimates for the coupled Biot model, we conclude that $\left\|\nabla \cdot \boldsymbol{u}_h^1 - \nabla \cdot \boldsymbol{u}_h^0\right\| \leq C\Delta t^2$ and $\left\|K^{-1/2}\boldsymbol{z}_h^1\right\|^2 \leq C$. This completes the derivation.

∎

Remark 3.2 The above proof also provides a way to devise an explicitly coupled algorithm that is unconditionally stable. For the single rate algorithm, we replace (2.4) by the following equation:
(**flow equation**) Find $p_h^{k+1} \in Q_h$ and $\boldsymbol{z}_h^{k+1} \in \boldsymbol{Z}_h$ such that,

$$\forall \theta_h \in Q_h, (\frac{1}{M} + c_f\varphi_0 + \frac{\alpha^2}{\lambda})\Big(\frac{p_h^{k+1} - p_h^k}{\Delta t}, \theta_h\Big) + \frac{1}{\mu_f}\Big(\nabla \cdot \boldsymbol{z}_h^{k+1}, \theta_h\Big) + \alpha\Big(\nabla \cdot \frac{\boldsymbol{u}_h^k - \boldsymbol{u}_h^{k-1}}{\Delta t}, \theta_h\Big) = \Big(\tilde{q}_h, \theta_h\Big). \tag{3.8}$$

Note that the stabilisation term $\frac{\alpha^2}{\lambda\Delta t}(p_h^{k+1} - p_h^k)$ has been added above in contrast to (2.4). The stability result is then obtained with the assumption ($\mathbf{A_1}$) relaxed. The consistence error is expected to be of order $O(\Delta t)$ which is also expected for the scheme.

To see the unconditional stability of the new scheme, consider the analog of (3.5) and proceed as in the previous case,

$$\begin{aligned}
&\frac{\beta + \frac{\alpha^2}{\lambda}}{\Delta t}\left\|p_h^{k+1} - p_h^k\right\|^2 + \frac{1}{2\mu_f}\left(\left\|K^{-1/2}\boldsymbol{z}_h^{k+1}\right\|^2 - \left\|K^{-1/2}\boldsymbol{z}_h^k\right\|^2 + \left\|K^{-1/2}(\boldsymbol{z}_h^{k+1} - \boldsymbol{z}_h^k)\right\|^2\right) \\
&+\frac{2G}{\Delta t}\left\|\boldsymbol{\varepsilon}(\boldsymbol{u}_h^{k+1} - \boldsymbol{u}_h^k)\right\|^2 + \frac{\lambda}{\Delta t}\left\|\nabla \cdot (\boldsymbol{u}_h^{k+1} - \boldsymbol{u}_h^k)\right\|^2 = \underbrace{-\frac{\alpha}{\Delta t}\Big(\nabla \cdot (\boldsymbol{u}_h^k - \boldsymbol{u}_h^{k-1}), p_h^{k+1} - p_h^k\Big)}_{R_1} \\
&+ \underbrace{\frac{\alpha}{\Delta t}\Big(p_h^{k+1} - p_h^k, \nabla \cdot (\boldsymbol{u}_h^{k+1} - \boldsymbol{u}_h^k)\Big)}_{R_2} + \underbrace{\Big(\tilde{q}_h, p_h^{k+1} - p_h^k\Big)}_{R_3} + \underbrace{\frac{1}{\Delta t}\Big(\boldsymbol{f}_h^{k+1} - \boldsymbol{f}_h^k, \boldsymbol{u}_h^{k+1} - \boldsymbol{u}_h^k\Big)}_{R_4}.
\end{aligned} \tag{3.9}$$

Denoting by R_1, R_2, R_3, and R_4 the terms on the right hand side, together with Poincaré's, Korn's, and Young's inequalities, we estimate

$$\begin{aligned}
|R_1| &\leq \frac{\alpha}{\Delta t}\frac{1}{2\epsilon_1}\left\|\nabla \cdot (\boldsymbol{u}_h^k - \boldsymbol{u}_h^{k-1})\right\|^2 + \frac{\alpha}{\Delta t}\frac{\epsilon_1}{2}\left\|p_h^{k+1} - p_h^k\right\|^2 \\
|R_2| &\leq \frac{\alpha}{2\Delta t\epsilon_2}\left\|\nabla \cdot (\boldsymbol{u}_h^{k+1} - \boldsymbol{u}_h^k)\right\|^2 + \frac{\alpha\epsilon_2}{2\Delta t}\left\|p_h^{k+1} - p_h^k\right\|^2 \\
|R_3| &\leq \frac{1}{2\epsilon_3}\left\|\tilde{q}_h\right\|^2 + \frac{\epsilon_3}{2}\left\|p_h^{k+1} - p_h^k\right\|^2 \\
|R_4| &\leq \frac{1}{2\Delta t\epsilon_4}\left\|\boldsymbol{f}_h^{k+1} - \boldsymbol{f}_h^k\right\|^2 + \frac{\epsilon_4}{2\Delta t}\left\|\boldsymbol{u}_h^{k+1} - \boldsymbol{u}_h^k\right\|^2 \\
&\leq \frac{1}{2\Delta t\epsilon_4}\left\|\boldsymbol{f}_h^{k+1} - \boldsymbol{f}_h^k\right\|^2 + \frac{\epsilon_4\mathcal{P}_\Omega^2 C_\kappa^2}{2\Delta t}\|\boldsymbol{\varepsilon}(\boldsymbol{u}_h^{k+1} - \boldsymbol{u}_h^k)\|^2.
\end{aligned}$$

for $\epsilon_1, \epsilon_2,$ and $\epsilon_4 > 0$. Choosing $\epsilon_1 = \frac{\alpha}{\lambda}$, $\epsilon_2 = \frac{\alpha}{\lambda}$, $\epsilon_3 = \frac{2\beta}{\Delta t}$, and $\epsilon_4 = \frac{2G}{\mathcal{P}_\Omega^2 C_\kappa^2}$ and multiplying (3.9) by $\frac{2\Delta t}{\lambda}$, we derive

$$\frac{\Delta t}{\lambda \mu_f}\Big(\Big\|K^{-1/2}\boldsymbol{z}_h^{k+1}\Big\|^2 - \Big\|K^{-1/2}\boldsymbol{z}_h^{k}\Big\|^2 + \Big\|K^{-1/2}(\boldsymbol{z}_h^{k+1} - \boldsymbol{z}_h^{k})\Big\|^2\Big) + \frac{2G}{\lambda}\Big\|\boldsymbol{\varepsilon}(\boldsymbol{u}_h^{k+1} - \boldsymbol{u}_h^{k})\Big\|^2$$
$$+\Big\|\nabla\cdot(\boldsymbol{u}_h^{k+1} - \boldsymbol{u}_h^{k})\Big\|^2 \leq \Big\|\nabla\cdot(\boldsymbol{u}_h^{k} - \boldsymbol{u}_h^{k-1})\Big\|^2 + \frac{\Delta t^2}{2\beta\lambda}\Big\|\tilde{q}_h\Big\|^2 + \frac{\mathcal{P}_\Omega^2 C_\kappa^2}{2G\lambda}\Big\|\boldsymbol{f}_h^{k+1} - \boldsymbol{f}_h^{k}\Big\|^2 \tag{3.10}$$

and rest of the steps proceeds as follows.

3.2 Multirate Formulation:

Recall that in the multirate explicit coupling approach, the flow problem is solved q times (with a finer time step) within a coarser mechanics time step.

Algorithm 2: Multirate Explicit Coupling Algorithm

Given initial conditions $\boldsymbol{u}_h^0$ *and* p_h^0, *solve implicitly for* $\boldsymbol{u}_h^m, p_h^m, \boldsymbol{z}_h^m, m = 1, 2, \ldots, q$ *satisfying fully coupled multirate Biot model*

for $k = q, 2q, 3q, ..$ **do** `/* mechanics time step iteration index */`

- First Step: Flow equations
- *Given* $\boldsymbol{u}_h^k$
- **for** $m = 1, 2, .., q$ **do** `/* flow finer time steps iteration index */`
  - *Solve for* p_h^{m+k} *and* $\boldsymbol{z}_h^{m+k}$ *satisfying definition 2.4*
- Second Step: Mechanics equations
- *Given* p_h^{k+q} *and,* $\boldsymbol{z}_h^{k+q}$
  - *Solve for* $\boldsymbol{u}_h^{k+q}$ *satisfying definition 2.5*

3.2.1 Assumptions

The stability assumption in the multirate case takes the form:

$$(\mathbf{A_q}) \quad \beta > \tfrac{1}{2}(\tfrac{1}{q} + q)\tfrac{\alpha^2}{\lambda} \qquad \text{for} \qquad q \geq 1,$$

where q is the number of flow finer time steps within one coarse mechanics time step.

As in the single rate case, we need to prepare the initial data for starting the time stepping. Accordingly, in the first step of the multirate algorithm (Algorithm 2), for $k = 0$, and $m = 1, 2, \ldots, q$, the initial conditions are computed by solving the coupled Biot system with fully implicit time discretization (with a time step of size Δt for the "q" coupled solves). Alternatively, decoupled iterative schemes [2,12] such as fixed stress iterative single rate scheme can be used to compute $\boldsymbol{u}_h^m, p_h^m, \boldsymbol{z}_h^m, m = 1, 2, \ldots, q$. Note that if $q = 1$, the multirate condition ($\mathbf{A_q}$) is identical to the single rate condition ($\mathbf{A_1}$).
Our main result is the following stability estimate.

Theorem 3.3 *[Multirate] Under the assumption* $(\mathbf{A_q})$, *the following stability result holds for the multirate explicit coupling scheme for mechanics time steps* $t_0 \leq t_k \leq t_J$, $k = q, 2q, ..$:

$$\frac{2G}{\lambda} \sum_{k=q}^{J} \left\| \boldsymbol{\varepsilon}(\boldsymbol{u}_h^{k+q} - \boldsymbol{u}_h^k) \right\|^2 + \frac{\Delta t}{\lambda \mu_f} \left(\left\| K^{-1/2} \boldsymbol{z}_h^{J+q} \right\|^2 + \sum_{k=q}^{J} \sum_{m=1}^{q} \left\| K^{-1/2}(\boldsymbol{z}_h^{m+k} - \boldsymbol{z}_h^{m-1+k}) \right\|^2 \right)$$
$$+ \left\| \nabla \cdot (\boldsymbol{u}_h^{J+q} - \boldsymbol{u}_h^J) \right\|^2 \leq C\Delta t + \frac{q\Delta t^2}{2\lambda\left(\beta - \frac{1}{2}(\frac{1}{q} + q)\frac{\alpha^2}{\lambda}\right)} \sum_{k=q}^{J} \left\| \tilde{q}_h \right\|^2 + \frac{\mathcal{P}_\Omega^2 C_\kappa^2}{2\lambda G} \sum_{k=q}^{J} \left\| \boldsymbol{f}_h^{k+q} - \boldsymbol{f}_h^k \right\|^2. \tag{3.11}$$

3.3 Stability Analysis

The proof for the stability analysis follows the same ideas as in the single rate proof, however the use of multiple time steps requires additional estimates. We follow the same principle of estimating the flow equation followed by mechanics equation and then combining the two together to obtain the stability estimates. *Proof.*

- **Step 1: Flow equations**
  Testing (2.7) with $\theta_h = p_h^{m+k} - p_h^{m-1+k}$, we get

$$\frac{\beta}{\Delta t} \left\| p_h^{m+k} - p_h^{m-1+k} \right\|^2 + \frac{1}{\mu_f} \left(\nabla \cdot \boldsymbol{z}_h^{m+k}, p_h^{m+k} - p_h^{m-1+k} \right)$$
$$+ \frac{\alpha}{q\Delta t} \left(\nabla \cdot (\boldsymbol{u}_h^k - \boldsymbol{u}_h^{k-q}), p_h^{m+k} - p_h^{m-1+k} \right) = \left(\tilde{q}_h, p_h^{m+k} - p_h^{m-1+k} \right) \tag{3.12}$$

In the flux equation (2.8), considering the difference for two consecutive finer time steps $t = t_{m+k}$ and $t = t_{m-1+k}$, and testing with $\boldsymbol{q}_h = \boldsymbol{z}_h^{m+k}$, we obtain

$$\left(K^{-1}(\boldsymbol{z}_h^{m+k} - \boldsymbol{z}_h^{m-1+k}), \boldsymbol{z}_h^{m+k} \right) = \left(p_h^{m+k} - p_h^{m-1+k}, \nabla \cdot \boldsymbol{z}_h^{m+k} \right). \tag{3.13}$$

Substituting (3.13) into (3.12), we derive

$$\beta \left\| p_h^{m+k} - p_h^{m-1+k} \right\|^2 + \frac{\Delta t}{\mu_f} \left(K^{-1}(\boldsymbol{z}_h^{m+k} - \boldsymbol{z}_h^{m-1+k}), \boldsymbol{z}_h^{m+k} \right)$$
$$= -\frac{\alpha}{q} \left(\nabla \cdot (\boldsymbol{u}_h^k - \boldsymbol{u}_h^{k-q}), p_h^{m+k} - p_h^{m-1+k} \right) + \Delta t \left(\tilde{q}_h, p_h^{m+k} - p_h^{m-1+k} \right)$$

Summing across flow finer time steps $1 \leq m \leq q$, we get (use $a(a-b) = \frac{1}{2}(a^2 - b^2 + (a-b)^2)$ and the telescopic cancellations)

$$\beta \sum_{m=1}^{q} \left\| p_h^{m+k} - p_h^{m-1+k} \right\|^2 + \frac{\Delta t}{2\mu_f} \left(\left\| K^{-1/2} \boldsymbol{z}_h^{k+q} \right\|^2 - \left\| K^{-1/2} \boldsymbol{z}_h^k \right\|^2 \right.$$
$$\left. + \sum_{m=1}^{q} \left\| K^{-1/2}(\boldsymbol{z}_h^{m+k} - \boldsymbol{z}_h^{m-1+k}) \right\|^2 \right) = -\frac{\alpha}{q} \left(\nabla \cdot (\boldsymbol{u}_h^k - \boldsymbol{u}_h^{k-q}), \sum_{m=1}^{q} (p_h^{m+k} - p_h^{m-1+k}) \right)$$
$$+ \Delta t \left(\tilde{q}_h, \sum_{m=1}^{q} (p_h^{m+k} - p_h^{m-1+k}) \right) \tag{3.14}$$

- **Step 2: Elasticity equation**
  Considering (2.9) for the difference of two consecutive mechanics time steps, $t = t_k$ and $t = t_{k+q}$, and testing with $\boldsymbol{v}_h = \boldsymbol{u}_h^{k+q} - \boldsymbol{u}_h^k$, we obtain

$$2G\Big\|\boldsymbol{\varepsilon}(\boldsymbol{u}_h^{k+q} - \boldsymbol{u}_h^k)\Big\|^2 + \lambda\Big\|\nabla\cdot(\boldsymbol{u}_h^{k+q} - \boldsymbol{u}_h^k)\Big\|^2 - \alpha(p_h^{k+q} - p_h^k, \nabla\cdot(\boldsymbol{u}_h^{k+q} - \boldsymbol{u}_h^k)) = \Big(\boldsymbol{f}_h^{k+q} - \boldsymbol{f}_h^k, \boldsymbol{u}_h^{k+q} - \boldsymbol{u}_h^k\Big). \tag{3.15}$$

- **Step 3: Combining flow and elasticity equations**
  Combining (3.14) with (3.15) gives

$$\begin{aligned}
&\beta\sum_{m=1}^{q}\Big\|p_h^{m+k} - p_h^{m-1+k}\Big\|^2 + 2G\Big\|\boldsymbol{\varepsilon}(\boldsymbol{u}_h^{k+q} - \boldsymbol{u}_h^k)\Big\|^2 + \lambda\Big\|\nabla\cdot(\boldsymbol{u}_h^{k+q} - \boldsymbol{u}_h^k)\Big\|^2 \\
&\quad + \frac{\Delta t}{2\mu_f}\Big(\Big\|K^{-1/2}\boldsymbol{z}_h^{k+q}\Big\|^2 - \Big\|K^{-1/2}\boldsymbol{z}_h^k\Big\|^2 + \sum_{m=1}^{q}\Big\|K^{-1/2}(\boldsymbol{z}_h^{m+k} - \boldsymbol{z}_h^{m-1+k})\Big\|^2\Big) \\
&= \underbrace{-\frac{\alpha}{q}\Big(\nabla\cdot(\boldsymbol{u}_h^k - \boldsymbol{u}_h^{k-q}), \sum_{m=1}^{q}(p_h^{m+k} - p_h^{m-1+k})\Big)}_{R_1} + \underbrace{\Delta t\Big(\tilde{q}_h, \sum_{m=1}^{q}(p_h^{m+k} - p_h^{m-1+k})\Big)}_{R_2} \\
&+ \underbrace{\alpha(p_h^{k+q} - p_h^k, \nabla\cdot(\boldsymbol{u}_h^{k+q} - \boldsymbol{u}_h^k))}_{R_3} + \underbrace{\Big(\boldsymbol{f}_h^{k+q} - \boldsymbol{f}_h^k, \boldsymbol{u}_h^{k+q} - \boldsymbol{u}_h^k\Big)}_{R_4}.
\end{aligned} \tag{3.16}$$

  Denoting by R_1 and R_2 the first two terms on the right hand side, Youngs's and triangle's inequalities give

$$\begin{aligned}
|R_1| &\leq \frac{\alpha}{q}\Big(\frac{\epsilon_1}{2}\sum_{m=1}^{q}\Big\|p_h^{m+k} - p_h^{m-1+k}\Big\|^2 + \frac{q}{2\epsilon_1}\Big\|\nabla\cdot(\boldsymbol{u}_h^k - \boldsymbol{u}_h^{k-q})\Big\|^2\Big), \\
|R_2| &\leq \Delta t\Big(\frac{\epsilon_2}{2}\sum_{m=1}^{q}\Big\|p_h^{m+k} - p_h^{m-1+k}\Big\|^2 + \frac{q}{2\epsilon_2}\Big\|\tilde{q}_h\Big\|^2\Big)
\end{aligned}$$

  Using the fact that $p_h^{k+q} - p_h^k = \sum_{m=1}^{q}\Big(p_h^{m+k} - p_h^{m-1+k}\Big)$ together with Young's and triangle's inequalities, the third term on the right hand side of (3.16), denoted by R_3, can be written as

$$|R_3| \leq \frac{\alpha\epsilon_3}{2}\sum_{m=1}^{q}\Big\|p_h^{m+k} - p_h^{m-1+k}\Big\|^2 + \frac{q\alpha}{2\epsilon_3}\Big\|\nabla\cdot(\boldsymbol{u}_h^{k+q} - \boldsymbol{u}_h^k)\Big\|^2 \tag{3.17}$$

By Poincaré's, Korn's, and Young's inequalities, the last term on the right hand side of (3.16), denoted by R_4, can be written as

$$
\begin{aligned}
|R_4| &\leq \frac{1}{2\epsilon_4}\left\|\boldsymbol{f}_h^{k+q}-\boldsymbol{f}_h^k\right\|^2+\frac{\epsilon_4}{2}\left\|\boldsymbol{u}_h^{k+q}-\boldsymbol{u}_h^k\right\|^2\\
&\leq \frac{1}{2\epsilon_4}\left\|\boldsymbol{f}_h^{k+q}-\boldsymbol{f}_h^k\right\|^2+\frac{\epsilon_4\mathcal{P}_\Omega^2C_\kappa^2}{2}\left\|\boldsymbol{\varepsilon}(\boldsymbol{u}_h^{k+q}-\boldsymbol{u}_h^k)\right\|^2.
\end{aligned}
$$

Choosing $\epsilon_1=\frac{\alpha}{\lambda}$, $\epsilon_2=\frac{2}{\Delta t}\Big(\beta-\frac{1}{2}(\frac{1}{q}+q)\frac{\alpha^2}{\lambda}\Big)$, $\epsilon_3=\frac{q\alpha}{\lambda}$, $\epsilon_4=\frac{2G}{\mathcal{P}_\Omega^2C_\kappa^2}$, and multiplying by $\frac{2}{\lambda}$ we derive

$$
\begin{aligned}
&\frac{\Delta t}{\lambda\mu_f}\left(\left\|K^{-1/2}\boldsymbol{z}_h^{k+q}\right\|^2-\left\|K^{-1/2}\boldsymbol{z}_h^k\right\|^2+\sum_{m=1}^{q}\left\|K^{-1/2}(\boldsymbol{z}_h^{m+k}-\boldsymbol{z}_h^{m-1+k})\right\|^2\right)\\
&\quad+\frac{2G}{\lambda}\left\|\boldsymbol{\varepsilon}(\boldsymbol{u}_h^{k+q}-\boldsymbol{u}_h^k)\right\|^2+\left\|\nabla\cdot(\boldsymbol{u}_h^{k+q}-\boldsymbol{u}_h^k)\right\|^2\leq\left\|\nabla\cdot(\boldsymbol{u}_h^k-\boldsymbol{u}_h^{k-q})\right\|^2\\
&\quad+\frac{q\Delta t^2}{2\lambda\Big(\beta-\frac{1}{2}(\frac{1}{q}+q)\frac{\alpha^2}{\lambda}\Big)}\left\|\tilde{q}_h\right\|^2+\frac{\mathcal{P}_\Omega^2C_\kappa^2}{2\lambda G}\left\|\boldsymbol{f}_h^{k+q}-\boldsymbol{f}_h^k\right\|^2.
\end{aligned}
\tag{3.18}
$$

We need to impose the following condition: $\beta-\frac{1}{2}(\frac{1}{q}+q)\frac{\alpha^2}{\lambda}>0$, which is nothing but the Assumption $\mathbf{A_q}$. Summing up equation (3.18) for $q\leq k\leq J$ (k is a multiple of q, that is, k = q, 2q, ..), we write

$$
\begin{aligned}
&\frac{2G}{\lambda}\sum_{k=q}^{J}\left\|\boldsymbol{\varepsilon}(\boldsymbol{u}_h^{k+q}-\boldsymbol{u}_h^k)\right\|^2+\frac{\Delta t}{\lambda\mu_f}\left(\left\|K^{-1/2}\boldsymbol{z}_h^{J+q}\right\|^2+\sum_{k=q}^{J}\sum_{m=1}^{q}\left\|K^{-1/2}(\boldsymbol{z}_h^{m+k}-\boldsymbol{z}_h^{m-1+k})\right\|^2\right)\\
&\quad+\left\|\nabla\cdot(\boldsymbol{u}_h^{J+q}-\boldsymbol{u}_h^J)\right\|^2\leq\frac{\Delta t}{\lambda\mu_f}\left\|K^{-1/2}\boldsymbol{z}_h^q\right\|^2+\left\|\nabla\cdot(\boldsymbol{u}_h^q-\boldsymbol{u}_h^0)\right\|^2\\
&\quad+\frac{q\Delta t^2}{2\lambda\Big(\beta-\frac{1}{2}(\frac{1}{q}+q)\frac{\alpha^2}{\lambda}\Big)}\sum_{k=q}^{J}\left\|\tilde{q}_h\right\|^2+\frac{\mathcal{P}_\Omega^2C_\kappa^2}{2\lambda G}\sum_{k=q}^{J}\left\|\boldsymbol{f}_h^{k+q}-\boldsymbol{f}_h^k\right\|^2.
\end{aligned}
\tag{3.19}
$$

To estimate the first two terms on the right hand side, we need to obtain a priori estimates for the fully implicit scheme for the multirate Biot. This a priori estimate is obtained by a slight variation of the technique from the single rate scheme and yields $\left\|\nabla\cdot(\boldsymbol{u}_h^q-\boldsymbol{u}_h^0)\right\|^2\leq Cq^2\Delta t^2$ and $\left\|K^{-1/2}\boldsymbol{z}_h^q\right\|\leq C$. We spare the details of obtaining these a priori estimates. Putting together, we conclude the result.

∎

Remark 3.4 As in the single rate case in remark 3.2, the multirate case can also be made unconditionally stable by adding a stabilisation term. In the definition 2.4, we modify the flow equation (2.7) by adding a stabilisation term $\gamma\frac{\alpha^2}{\lambda\Delta t}(p_h^{m+k}-p_h^{m-1+k})$, where $\gamma=\frac{1}{2}(\frac{1}{q}+q)$. The modified equation reads:

(**flow equation**) For $1 \le m \le q$, find $p_h^{m+k} \in Q_h$, and $\boldsymbol{z}_h^{m+k} \in \boldsymbol{Z}_h$ such that,

$$\forall \theta_h \in Q_h\,, \frac{1}{\Delta t}\Big((\frac{1}{M} + c_f \varphi_0 + \frac{\gamma\alpha^2}{\lambda})\Big(p_h^{m+k} - p_h^{m-1+k}\Big), \theta_h\Big) + \frac{1}{\mu_f}(\nabla \cdot \boldsymbol{z}_h^{m+k}, \theta_h) = \\ - \frac{\alpha}{q\Delta t}\Big(\nabla \cdot \Big(\boldsymbol{u}_h^k - \boldsymbol{u}_h^{k-q}\Big), \theta_h\Big) + \Big(\tilde{q}_h, \theta_h\Big). \tag{3.20}$$

The proof for the unconditional stability follows the same ideas as in the single rate case and is skipped here.

Remark 3.5 For the numerical simulations we will be using the multipoint flux mixed finite element method (MFMFE) [22,23] for the flow discretization. All our obtained results remain valid for this discretization. Indeed, for such a scheme, the stability results (3.19) translates to,

$$\frac{\Delta t}{\lambda \mu_f}\Big(K^{-1}\boldsymbol{z}_h^{J+q}, \boldsymbol{z}_h^{J+q}\Big)_Q + \frac{\Delta t}{\lambda \mu_f}\sum_{k=q}^{J}\sum_{m=1}^{q}\Big(K^{-1}(\boldsymbol{z}_h^{m+k} - \boldsymbol{z}_h^{m-1+k}), (\boldsymbol{z}_h^{m+k} - \boldsymbol{z}_h^{m-1+k})\Big)_Q \\ + \frac{2G}{\lambda}\sum_{k=q}^{J}\Big\|\varepsilon(\boldsymbol{u}_h^{k+q} - \boldsymbol{u}_h^k)\Big\|^2 + \Big\|\nabla \cdot (\boldsymbol{u}_h^{J+q} - \boldsymbol{u}_h^J)\Big\|^2 \le \frac{\Delta t}{\lambda \mu_f}\Big(K^{-1}\boldsymbol{z}_h^q, \boldsymbol{z}_h^q\Big)_Q \tag{3.21} \\ + \Big\|\nabla \cdot (\boldsymbol{u}_h^q - \boldsymbol{u}_h^0)\Big\|^2 + \frac{q\Delta t^2}{2\lambda\Big(\beta - \frac{1}{2}(\frac{1}{q} + q)\frac{\alpha^2}{\lambda}\Big)}\sum_{k=q}^{J}\Big\|\tilde{q}_h\Big\|^2 + \frac{\mathcal{P}_\Omega^2 C_\kappa^2}{2\lambda G}\sum_{k=q}^{J}\Big\|\boldsymbol{f}_h^{k+q} - \boldsymbol{f}_h^k\Big\|^2,$$

where $(K^{-1}.,.)_Q$ is the quadrature rule defined in [23] for the MFMFE corresponding spaces. It was shown by Wheeler and Yotov in [23], and then extended to distorted quadrilaterals and hexahedra in [22], that for any $\boldsymbol{z}_h \in \boldsymbol{Z}_h, C_1\|\boldsymbol{z}_h\|^2 \le (K^{-1}\boldsymbol{z}_h, \boldsymbol{z}_h)_Q \le C_2\|\boldsymbol{z}_h\|^2$, for a constant $C_1, C_2 > 0$. This immediately leads to a similar stability result. The same argument holds for single rate case.

Remark 3.6 The well source/sink term ($\tilde{q}_h$) can be assumed to be varying with discrete fine/coarse time steps, and all obtained results remain valid.

4 Numerical Results

4.1 Iterative vs. Explicit Coupling Schemes

In this section, we compare single rate and multirate explicit coupling schemes versus iterative coupling schemes. Both schemes are implemented in the Integrated Parallel Accurate Reservoir Simulator (IPARS) on top of a single-phase flow model coupled with a linear poroelasticity model. The Multipoint Flux Mixed Finite Element Method (MFMFE) is used for flow discretization and Conformal Galerkin is used for elasticity discretization. Mikelić and Wheeler [15] have analyzed different iterative coupling schemes, and have shown that the two often used techniques known as the fixed-stress split and the undrained-split coupling algorithms are unconditionally stable. The numerical computations in [14] show the relative performances of the two methods with fixed stress splitting performing better.

Total Simulation time:	64.0 days	k_{xx}	Range: (0.002122, 350.1372) md
Finer (Unit) time step:	1.0 days	k_{yy}	Range: (0.022143, 4135.124) md
Number of grids:	60048 grids (9×48×139)	k_{zz}	Range: (0.022493, 4163.053) md
Possion Ratio, ν	0.35	Biot Modulus, M	1.E15 psi
Biot's constant, α	0.9	$\lambda = \frac{E\nu}{(1+\nu)(1-2\nu)}$	4.32E7 psi
Initial porosity, φ_0	0.2	Flow Boundary Conditions:	zero flow B.C.
Fluid viscosity, μ_w	1.0 cp	Mechanics B.C.:	
Initial fluid pressure, p_0	1000.0 psi	"X+" boundary	$\sigma_{xx} = \sigma \cdot n_x = 10,000psi$
fluid compressibility c_{f_w}:	1.E-6 (1/psi)	"X-" - boundary	$\boldsymbol{u} = 0$, zero displacement
Rock compressibility:	1.E-6 (1/psi)	"Y+" - boundary	$\boldsymbol{u} = 0$, zero displacement
Rock density:	165.44 lb_m/ft^3	"Y-" - boundary	$\sigma_{yy} = \sigma \cdot n_y = 2000psi$
Initial fluid density, ρ_o	62.34 lb_m/ft^3	"Z+" - boundary	$\boldsymbol{u} = 0$, zero displacement
Young's Modulus (E)	5.0E7 psi	"Z-" - boundary	$\sigma_{zz} = \sigma \cdot n_z = 1000psi$

Table 1: Input Parameters for Brugge Field Model

% of Reduction in:	$q = 1$	$q = 2$	$q = 4$	$q = 8$
CPU run time	47.34%	47.62%	44.97%	51.69%
Number of flow linear iterations	48.50%	52.92%	52.16%	53.55%
Number of mechanics linear iterations	52.21%	52.20%	51.50%	52.89%

Table 2: Computational savings of explicit coupling schemes versus iterative coupling schemes for different values of "q" (the number of flow fine time steps within one coarse mechanics time step).

In the multirate case the unconditional stability of these two schemes have been studied in [2, 12]. For our numerical tests, we consider the iterative fixed-stress coupling algorithm when comparing the efficiency of the iterative coupling schemes versus explicit coupling schemes.

4.1.1 Brugge Fileld Model

We consider the Brugge field model [19] for comparing the accuracy and efficiency of iterative versus explicit coupling schemes. The model consists of a 9 × 48 × 139 general hexahedral elements capturing the field geometry, with 30 bottom-hole pressure specified wells, 10 of which are injectors at a pressure of 4600 psi, and 20 are producers at a pressure of 1200 psi. Producers are located at a lower elevation compared to injectors. No flow boundary condition is enforced across all external boundaries. For the mechanics model, we apply a mixture of zero displacement and traction boundary conditions. we also include the effects of gravity. Detailed specifications of the input parameters can be found in Table 1. We note here that assumptions ($\mathbf{A_1}$) and ($\mathbf{A_q}$) are both satisfied for the single rare and multirate explicit coupling cases ($q = 1, 2, 4$, and 8), respectively.

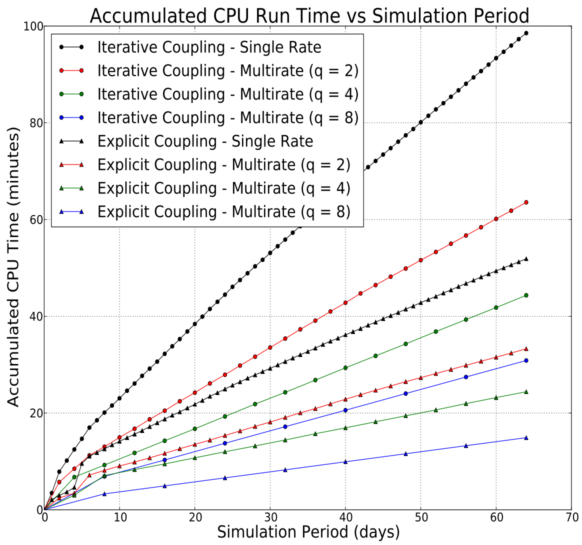

(a) CPU Run Time vs Simulation Days

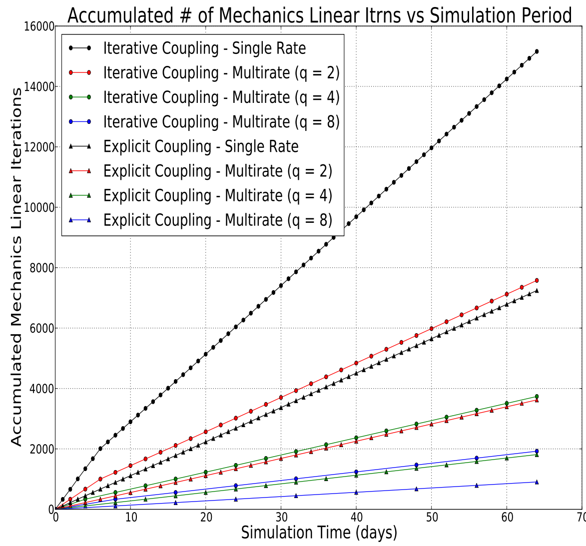

(b) Total Number of Mechanics Linear Iterations vs Simulation Days

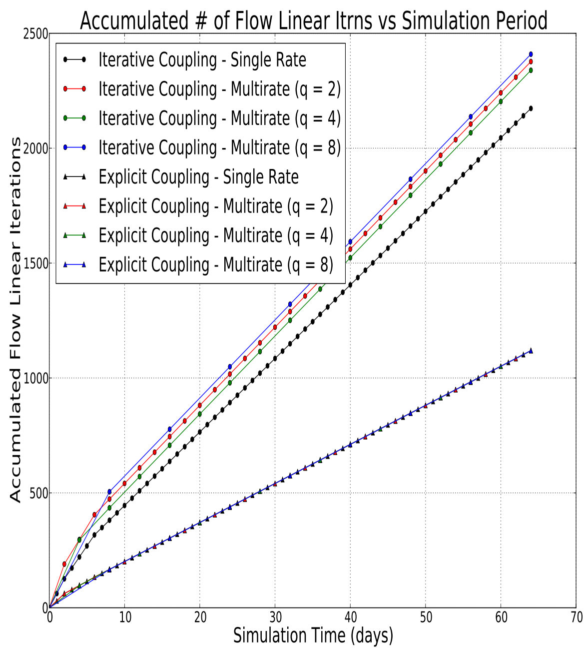

(c) Total Number of Flow Linear Iterations vs Simulation Days

Figure 4.1: Brugge Field Model Numerical Results

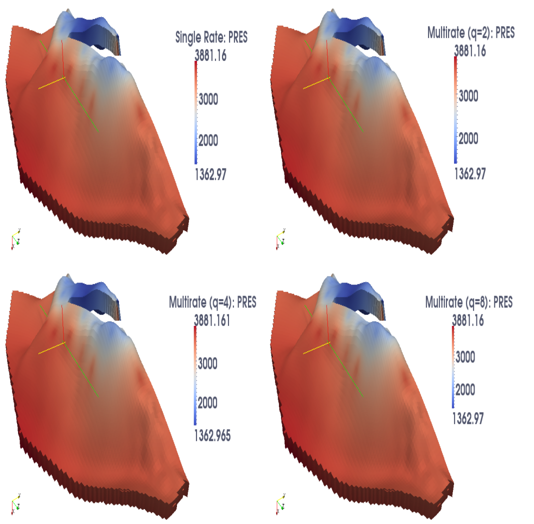

(a) Pressure field at 64.0 days (Iterative Coupling)

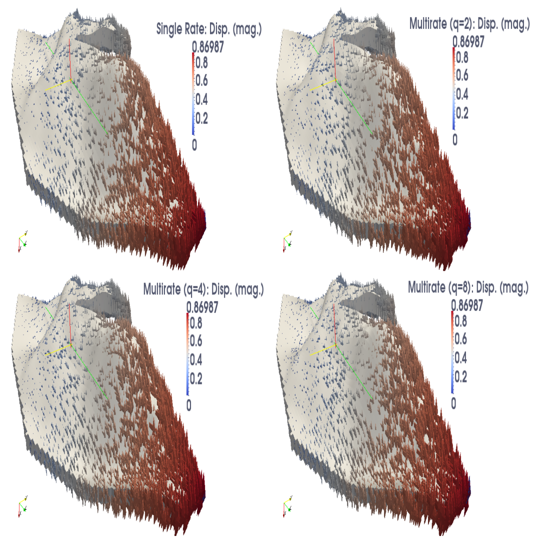

(b) Displacement field at 64.0 days (Iterative Coupling)

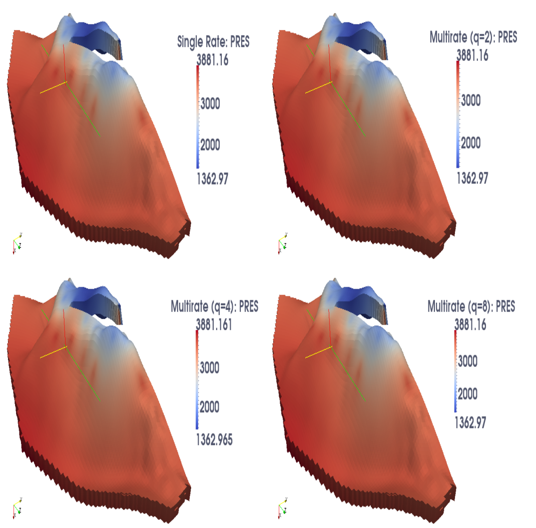

(c) Pressure field at 64.0 days (Explicit Coupling)

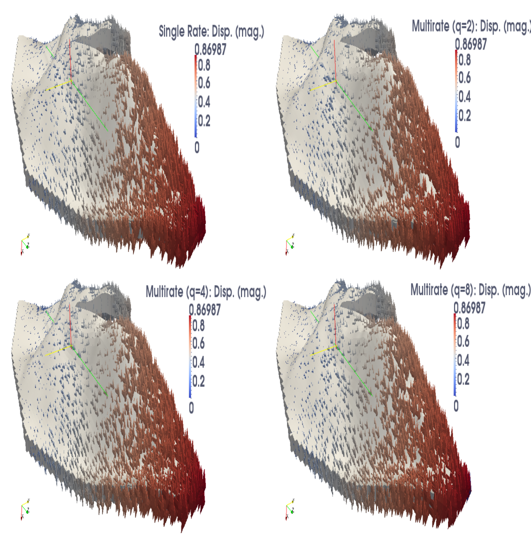

(d) Displacement field at 64.0 days (Explicit Coupling)

Figure 4.2: Iterative vs Explicit Coupling Results: Background: Pressure Profile, Arrows: Mechanical Displacements

4.1.2 Results & Discussion

Figure 4.1a shows the accumulated CPU run time for the single rate case ($q = 1$), and for multirate cases: $q = 2$, 4, and 8, for both iterative and explicit coupling schemes. In general, for a fixed q, explicit coupling schemes are more efficient, compared to their counterpart iterative coupling schemes. This is expected as explicit schemes eliminate any coupling iteration between the two problems. This results in a huge reduction in the total number of flow and mechanics linear iterations for explicit coupling schemes, as shown in Figures 4.1c, and 4.1b respectively. The results obtained show that explicit coupling schemes can reduce the accumulative number of flow linear iterations for the whole simulation run by almost 50.0% compared to iterative coupling schemes. In addition, the accumulative number of mechanics linear iterations is reduced as well when comparing an explicit coupling scheme to an iterative scheme for a fixed value of q. As shown in figure 4.1b, the single rate iterative coupling scheme results in the highest number of total mechanics linear iterations. In contrast, the multirate explicit coupling scheme (q=8) results in the lowest number of mechanics linear iterations for the whole simulation run. Computational savings of explicit coupling schemes versus iterative coupling schemes are shown in Table 2.

Figures 4.2a and 4.2b show the pressure and displacement fields for the iterative coupling scheme after 64.0 days of simulation of the Brugge field case. Figures 4.2c and 4.2d show the corresponding fields for the explicit coupling scheme. The solutions for both the approaches are fairly close with a slight difference between the iterative and explicit coupling being more apparent for pressure fields. The differences in displacement fields for both schemes are negligible.

4.2 Validating Theoretical Assumptions

In this section, we try to validate our theoretically induced assumptions for the single rate and multirate explicit coupling schemes against the Frio field model. Located on the Gulf Coast, near Dayton, Texas, at South Liberty oil field, the Frio field model is a field-scale problem with a geometrically challenging geological formation [9]. The field is curved in the depth direction, with several thin curved faults [9]. In this work, we only consider the challenging geometry of the field, and its real permeability distribution. Gravity effects are included in this model. Other input specifications are shown in Table 3.

4.2.1 Results & Discussion

We recall that for the single rate case, the stability assumption is $(\frac{1}{M} + c_f\varphi_0) > \frac{\alpha^2}{\lambda}$ and in the multirate case it reads $(\frac{1}{M} + c_f\varphi_0) > \frac{1}{2}(\frac{1}{q} + q)\,\frac{\alpha^2}{\lambda}$. We consider a particular choice for $q = 2$ and for the parameters shown in Table 3, our assumption requires $(\frac{1}{M} + c_f\varphi_0) > (1.06 \times 10^{-5})$. For the numerical test cases, we consider two different compressibility values corresponding to (1) satisfying the stability condition and (2) the stability assumption is violated.

In the first case, we choose $c_f = 1.0 \times 10^{-4}$ satisfying the stability assumption. The pressure profile after 4010 simulation days is shown in figure 4.3a. Resulting pressures lie

Wells:	3 production wells, 6 injection well
Injection well (1): Injection well (2): Injection well (3): Injection well (4): Injection well (5): Injection well (6): Production well (1): Production well (2): Production well (3):	Pressure specified, 14000.0 psi Pressure specified, 8300.0 psi Pressure specified, 8000.0 psi Pressure specified, 8400.0 psi Pressure specified, 8700.0 psi Pressure specified, 4400.0 psi Pressure specified, 2000.0 psi Pressure specified, 2000.0 psi Pressure specified, 2000.0 psi
Total Simulation time:	4010.0 days
Finer flow (Unit) time step:	1.0 days
Coarse mechanics time step:	2.0 days (q = 2)
Number of grids:	891 grids (33 × 9 × 3)
Permeabilities: k_{xx}, k_{yy}, k_{zz}	highly varying, range: (5.27E-10, 3.10E+3) md
Initial porosity, φ_0:	0.2
Fluid viscosity, μ_f:	1.0 cp
Initial pressure, p_0:	400.0 psi
Fluid compressibilities:	
Case (1), condition is satisfied, c_f:	1.E-4 (1/psi)
Case (2), condition is not satisfied, c_f:	1.E-13 (1/psi)
Case (3), condition is not satisfied, c_f:	1.E-8 (1/psi)
Rock compressibility:	1.E-6 (1/psi)
Rock density:	165.44 lb_m/ft^3
Initial fluid density, ρ_f:	62.34 lb_m/ft^3
Young's Modulus (E):	1.E5 psi
Possion Ratio, ν:	0.3
Biot's constant, α:	0.7
Biot Modulus, M:	1.0E16 psi
$\lambda = \frac{E\nu}{(1+\nu)(1-2\nu)}$:	57692.3 psi
Flow Boundary Conditions:	no flow boundary condition on all 6 boundaries
Mechanics B.C.:	
"X+" boundary (EBCXX1()):	$\sigma_{xx} = \sigma \cdot n_x = 10,000psi$, (overburden pressure)
"X-" - boundary (EBCXXN1()):	$\boldsymbol{u} = 0$, zero displacement
"Y+" - boundary (EBCYY1()):	$\boldsymbol{u} = 0$, zero displacement
"Y-" - boundary (EBCYYN1()):	$\sigma_{yy} = \sigma \cdot n_y = 2000psi$
"Z+" - boundary (EBCZZ1()):	$\boldsymbol{u} = 0$, zero displacement
"Z-" - boundary (EBCZZN1()):	$\sigma_{zz} = \sigma \cdot n_z = 1000psi$

Table 3: Input Parameters for Frio Field Model

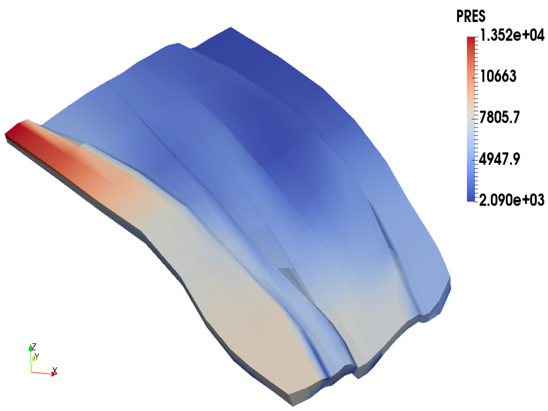

(a) Pressure profile when the compressibility of the fluid satisfies the derived stability condition ($c_f = 1 \times 10^{-4}$).
Results are physically correct, and lie between the expected range of values.

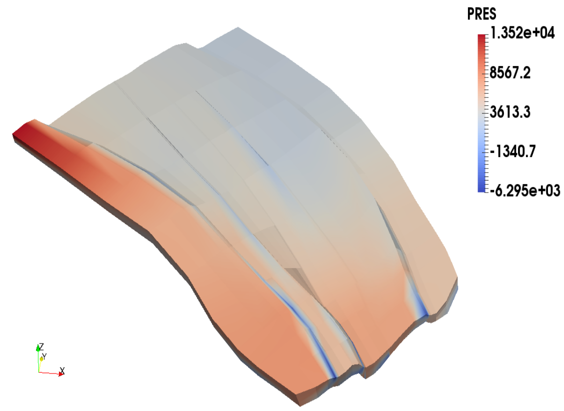

(b) Pressure profile when the compressibility of the fluid does not satisfy the derived stability condition ($c_f = 1 \times 10^{-8}$). Results are not physically correct, as pressure values drop below zero.

Figure 4.3: Pressure profiles of the multirate explicit coupling scheme (q=2) for the Frio field model.

in the expected range of values, based on wells' injection and production rates specified in table 3.
Next, we consider the case when we choose $c_f = 1.0 \times 10^{-13}$, that strongly violates the stability condition. In this case, the coupling iteration did not converge, as a result of producing extremely high pressure values (in magnitudes), and that, in turn, triggered the pore-volume values of grid blocks to exceed their corresponding bulk-volume values, which is physically meaningless. To further test the effect of compressibility, we increase the compressibility and choose ($c_f = 1.0 \times 10^{-8}$ (still violating the stability condition). In this case, the pressure profiles after 4010 simulation days are shown for two compressibilities (in figure 4.3b. It is clear from the figure that the pressure profiles are unphysical since the pressure values drop below zero. Given the values of the initial pressure, and wells' injection and production rates specified in table 3, this is a non-physical solution.

5 Conclusions and outlook

In this work, we considered single rate and multirate explicit coupling schemes for coupling flow with geomechanics in poro-elastic media. We derived stability criteria for both multirate and single rate schemes and derived the assumptions on reservoir parameters for the stability to hold. In addition, we perform the numerical experiments where we compare the time savings in the explicit coupling schemes compared to the iterative fixed stress schemes. The multirate iterative schemes have been proven to be geometrically convergent. Our computational results show that, if the parameters satisfy the stability condition, explicit coupling schemes reduce CPU run time efficiently as compared to iterative schemes.

Acknowledgements

TA is funded by Saudi Aramco. We thank Paulo Zunino and Ivan Yotov for helpful discussions. KK would like to acknowledge the support of Statoil Akademia Grant (Bergen). The authors would like to acknowledge the CSM Industrial Affiliates program, DOE grant ER25617, and ConocoPhillips grant UTA10-000444.

References

[1] T. Almani, A. H. Dogru, K. Kumar, G. Singh, and M. F. Wheeler. Convergence of multirate iterative coupling of geomechanics with flow in a poroelastic medium. *Saudi Aramco Journal of Technology*, Spring 2016.

[2] T. Almani, K. Kumar, A. H. Dogru, G. Singh, and M. F. Wheeler. Convergence analysis of multirate fixed-stress split iterative schemes for coupling flow with geomechanics. Ices report 16-07, Institute for Computational Engineering and Sciences, The University of Texas at Austin, Austin, Texas, 2016.

[3] M. A. Biot. Consolidation settlement under a rectangular load distribution. *J. Appl. Phys.*, 12(5):426–430, 1941.

[4] M. A. Biot. General theory of three-dimensional consolidation. *J. Appl. Phys.*, 12(2):155–164, 1941.

[5] L. Y. Chin, L. K. Thomas, J. E. Sylte, and R. G. Pierson. Iterative coupled analysis of geomechanics and fluid flow for rock compaction in reservoir simulation. *Oil and Gas Science and Technology*, 57(5):485–497, 2002.

[6] O. Coussy. *Mechanics of Porous Continua*. Wiley, West Sussex PO19 1UD, England, 1995.

[7] X. Gai, R. H. Dean, M. F. Wheeler, and R. Liu. Coupled geomechanical and reservoir modeling on parallel computers. In *The SPE Reservoir Simulation Symposium, Houston, Texas*, Feb. 3-5, 2003.

[8] V. Girault, M. F. Wheeler, B. Ganis, and M. Mear. A lubrication fracture model in a poro-elastic medium. Technical report, The Institute for Computational Engineering and Sciences, The University of Texas at Austin, 2013.

[9] M. Juntunen and M. F. Wheeler. Two-phase flow in complicated geometries - modeling the frio data using improved computational meshes. *Computational Geosciences*, 17:239–247, 2013.

[10] J. Kim, H. A. Tchelepi, and R. Juanes. Stability and convergence of sequential methods for coupled flow and geomechanics: fixed-stress and fixed-strain splits. *Comput. Methods Appl. Mech. Engrg.*, 200(13-16):1591–1606, 2011.

[11] J. Kim, H. A. Tchelepi, and R. Juanes. Stability, accuracy, and efficiency of sequential methods for coupled flow and geomechanics. In *The SPE Reservoir Simulation Symposium, Houston, Texas*, February 2-4, 2009. SPE119084.

[12] K. Kumar, T. Almani, G. Singh, and M. F. Wheeler. Multirate undrained splitting for coupled flow and geomechanics in porous media. In *ENUMATH 2015 Proceedings*. European Conference on Numerical Mathematics and Advanced Applications, September 14-18, 2015. submitted.

[13] M. Mainguy and P. Longuemare. Coupling fluid flow and rock mechanics: formulations of the partial coupling between reservoir and geomechanics simulators. *Oil and Gas Science and Technology - Rev. IFP*, 57(4):355–367, 2002.

[14] A. Mikelić, B. Wang, and M. F. Wheeler. Numerical convergence study of iterative coupling for coupled flow and geomechanics. *Computational Geosciences*, 18:325–341, 2014.

[15] A. Mikelić and M. F. Wheeler. Convergence of iterative coupling for coupled flow and geomechanics. *Computational Geosciences*, 17:455–461, 2013.

[16] P. Samier, A. Onaisi, and S. d. Gennaro. A practical iterative scheme for coupling geomechanics with reservoir simulation. *SPE Reservoir Evaluation and Engineering*, 11:892–901.

[17] A. Settari and F. M. Mourits. Coupling of geomechanics and reservoir simulation models. In Siriwardane and Zema, editors, *Comp. Methods and Advances in Geomech.*, pages 2151–2158, Balkema, Rotterdam, 1994.

[18] L. Shan, H. Zheng, and W. J. Layton. A decoupling method with different subdomain time steps for the nonstationary stokes-darcy model. *Numerical Methods for Partial Differential Equations*, 29(2):549–583, 2013.

[19] G. Singh. *Coupled Flow and Geomechanics Modeling for Fractured Poroelastic Reservoirs*. PhD thesis, The University of Texas at Austin, Austin, Texas, 2014.

[20] J. C. Small, J. R. Booker, and E. H. Davis. Elasto-plastic consolidation of soil. *Int. J. Solids Struct.*, 12(6):431–448, 1976.

[21] K. V. Terzaghi. *Theoretical Soil Mechanics*. Wiley, New York, 1943.

[22] M. F. Wheeler, G. Xue, and I. Yotov. A multipoint flux mixed finite element method on distorted quadrilaterals and hexahedra. *Numerische Mathematik*, 121(1):165–204, 2012.

[23] M. F. Wheeler and I. Yotov. A multipoint flux mixed finite element method. *SIAM Journal of Numerical Analysis*, 44:2082–2106, 2006.

[24] X. Xiong. *Partitioned methods for coupled fluid flow and turbulence flow problems*. PhD thesis, University of Pittsburgh, Pittsburgh, Pennsylvania, 2014.